Supplementary Figures (1 PDF file)

Identification of Targetable FGFR Gene Fusions in Diverse Cancers

Yi-Mi Wu, Fengyun Su, Shanker Kalyana-Sundaram, Nick Khazanov, Bushra Ateeq, Xuhong Cao, Robert J. Lonigro, Pankaj Vats, Rui Wang, Su-Fang Lin, Ann-Joy Cheng, Lakshmi P. Kunju, Javed Siddiqui, Scott A. Tomlins, Peter Wyngaard, Seth Sadis, Sameek Roychowdhury, Maha H. Hussain, Felix Feng, Mark M. Zalupski, Moshe Talpaz, Kenneth J. Pienta, Daniel R. Rhodes, Dan R. Robinson, and Arul M. Chinnaiyan

Supplementary Figures S1-S9 show the phenotypic effects and signaling pathways of FGFR fusions *in vitro* and *in vivo*.

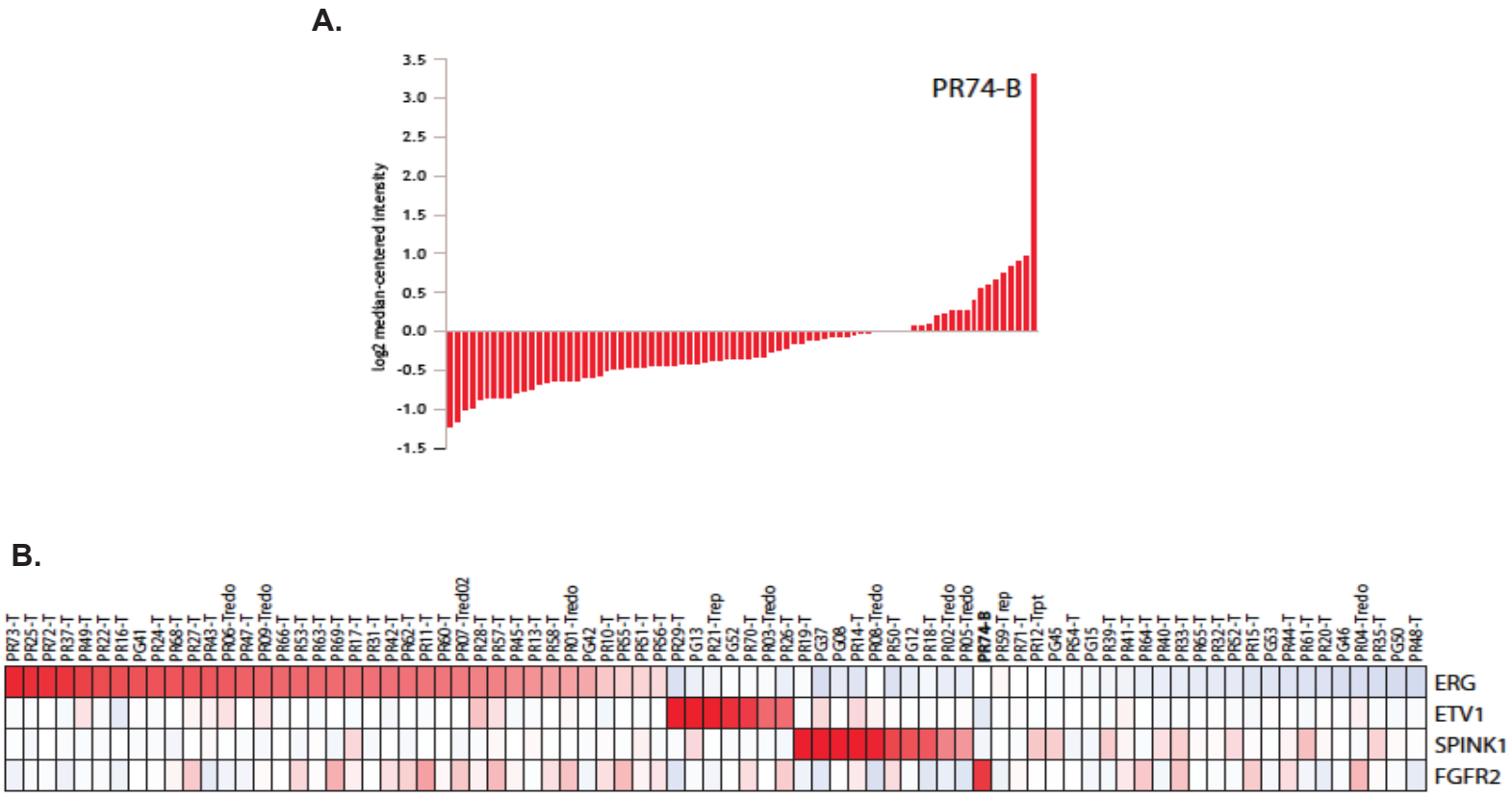

Supplementary Figure S1. Rare *FGFR2* outlier expression in an ETS fusion(-) / SPINK1(-) aggressive prostate cancer. *FGFR2* expression was assessed across prostate cancer (PCa) profiling studies in the Oncomine database. **A.** A single localized PCa with outlier *FGFR2* expression (PR74-B) was identified in the Glinsky *et al.* prostate profiling study. PR74-B was obtained from a 72 year old man with a Gleason score 9 PCa with extraprostatic extension on radical prostatectomy. **B.** Heatmap of ETS genes involved in recurrent fusions (*ERG* and *ETV1*), *SPINK1* and *FGFR2* in the Glinksky *et al.* study demonstrates that PR74-B is ETS fusion-/SPINK1- based on outlier expression.

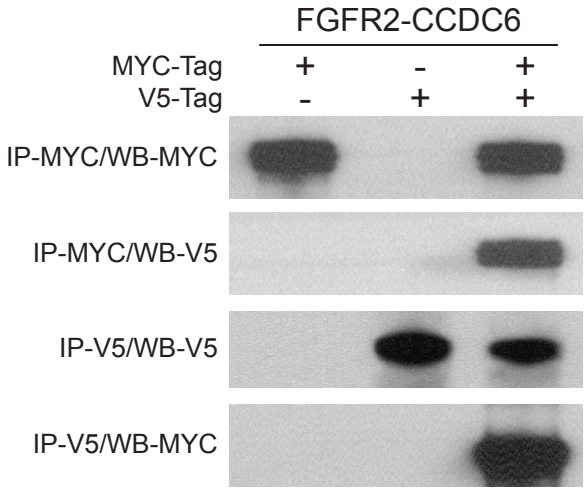

Supplementary Figure S2. **Detection of dimerization FGFR fusion proteins by immuno-precipitation (IP)-Western blotting (WB).** cDNA encoding the *FGFR2-CCDC6* fusion allele was cloned into pcDNA3.1 vectors with either MYC-epitope tag or V5-epitope tag attached to the C-terminus of expressed protein. The expression constructs were transfected into 293T cells alone or in combination of both tagged versions. Protein lysates were immunoprecipitated and immunoblotted with antibodies indicated on the left side of the images.

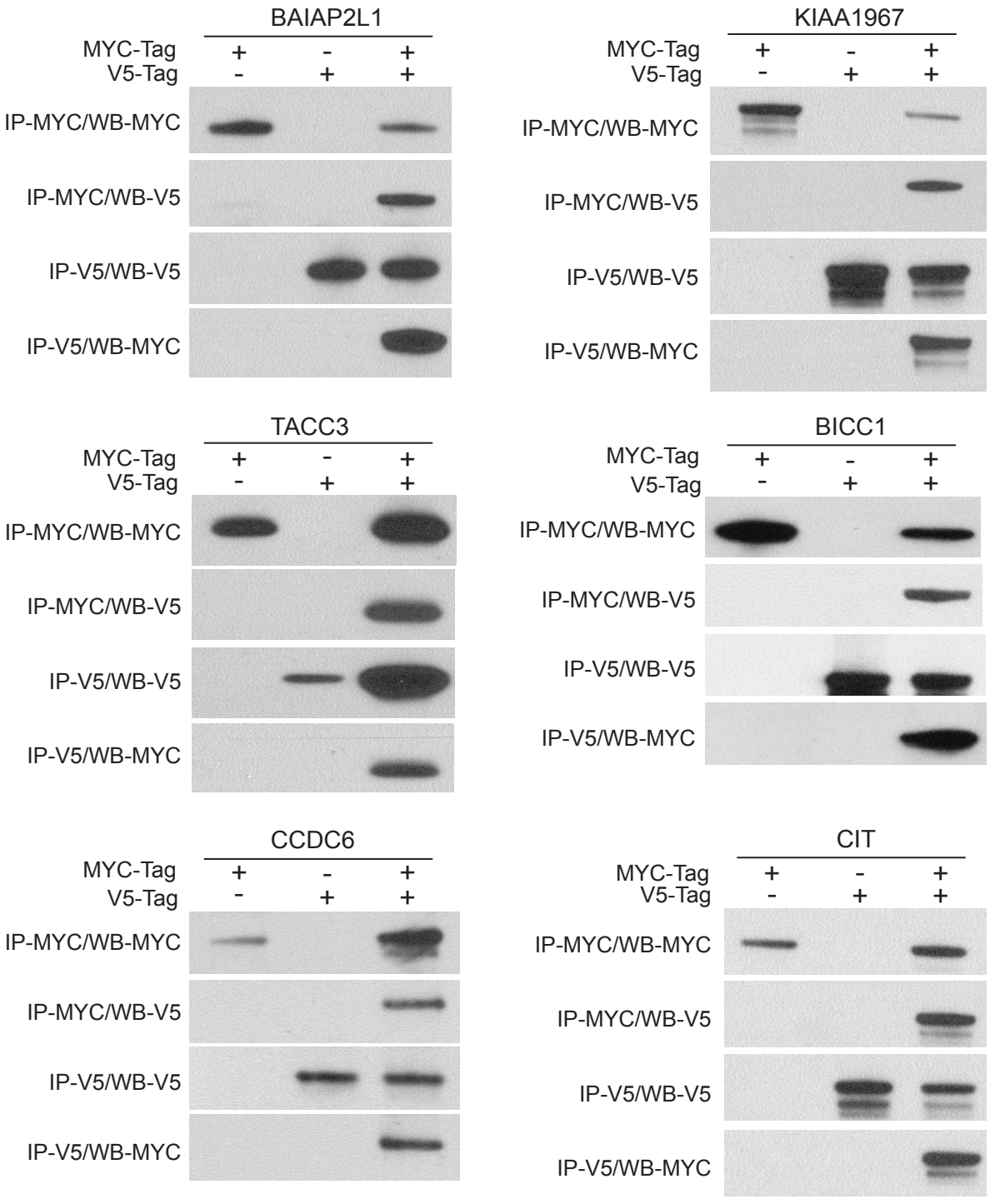

Supplementary Figure S3. **Dimerization of FGFR fusion partners as measured by immunoprecipitation (IP)-Western blotting (WB).** cDNAs encoding the C-terminal domains contributed by the 3' genes of 6 different FGFR fusions were cloned into pcDNA3.1 vectors with either MYC-epitope tag or V5-epitope tag at the C-terminus. The expression constructs were transfected into 293T cells alone or in combination. Protein lysates were immunoprecipitated and immunoblotted with epitope-specific antibodies as indicated on the left of the images.

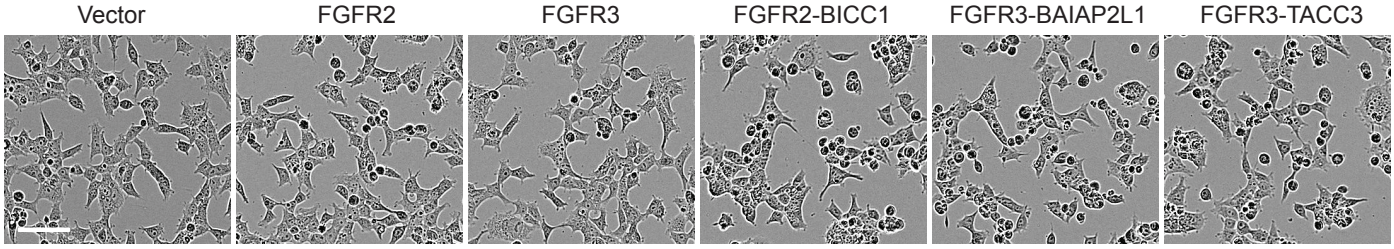

Supplementary Figure S4. **Morphologic changes in 293T cells over-expressing FGFR fusion proteins.** HEK 293T cells were transfected with respective FGFR wild-type or fusion constructs**.** Cell morphology was recorded under microscope. Scale bar, 100 um.

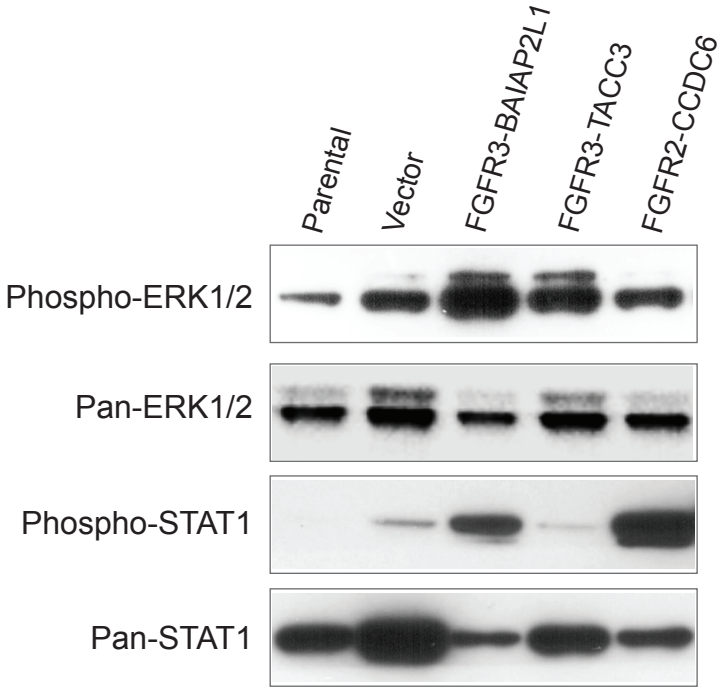

Supplementary Figure S5. Activation of MAPK and STAT1 by FGFR fusion proteins in TERT-HME cells. Lysates of breast TERT-HME cells (parental), stable lines overexpressing various FGFR fusions, or vector control, were analyzed by Western blotting using phospho-ERK1/2, pan-ERK1/2, phospho-STAT1, and pan-STAT1 antisera.

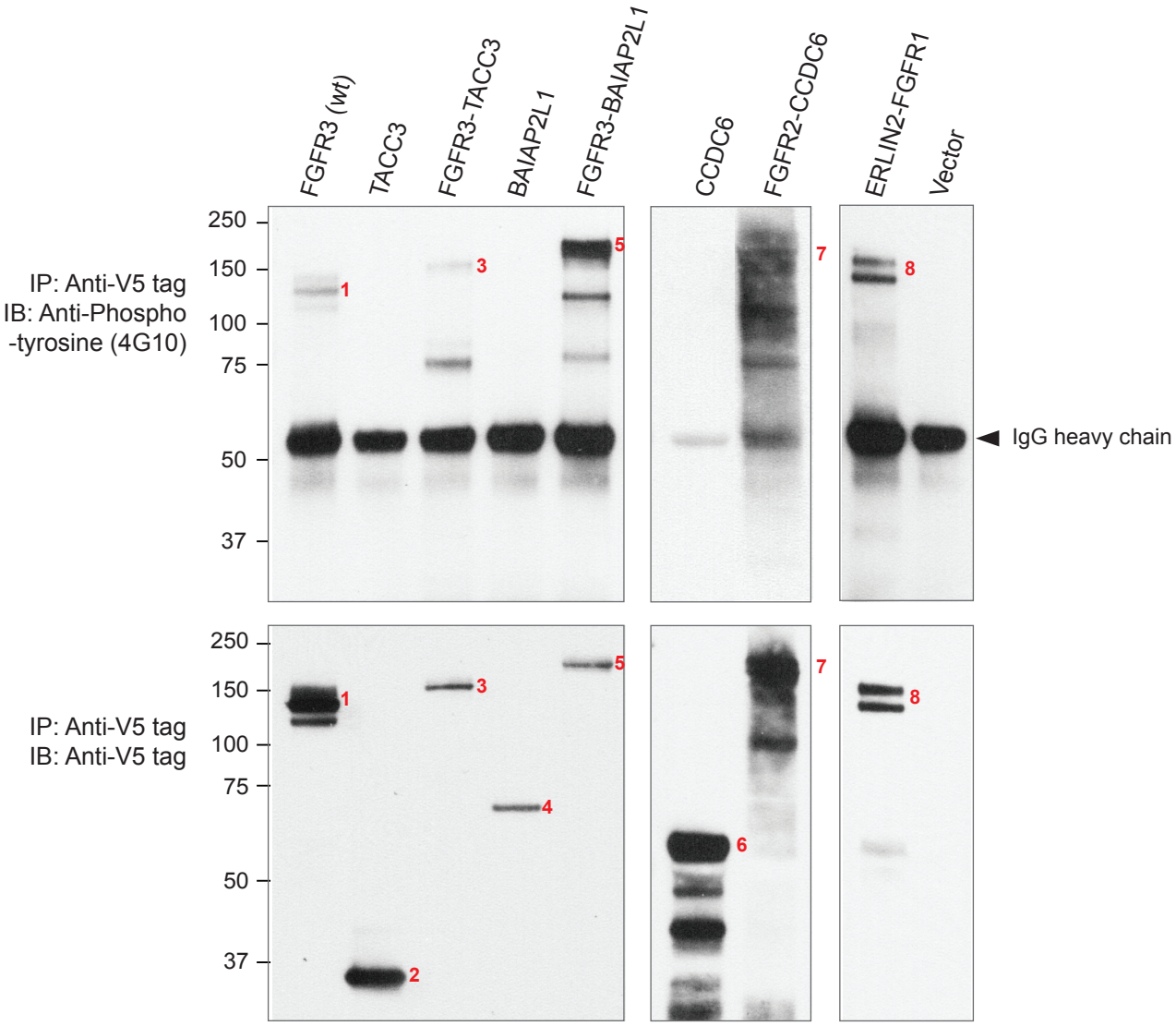

Supplementary Figure S6. Detection of phophorylated FGFR fusion proteins ectopically expressed in 293T cells. 293T cells were transfected with vector, wild-type (wt) FGFR3, various FGFR fusions, or FGFR fusion partners alone. Cell lysates were immunoprecipitated (IP) with anti-V5 tag antibody, and immunoblotted (IB) with anti-V5 antibody or anti-phospho-tyrosine antibody (4G10). Numbers indicate positions of recombinant proteins. Predicted protein sizes: FGFR3, 108 kDa; TACC3, 26 kDa; FGFR3-TACC3 fusion, 120 kDa; BAIAP2L1, 56 kDa; FGFR3-BAIAP2L1 fusion, 152 kDa; CCDC6, 40 kDa; FGFR2-CCDC6 fusion, 120 kDa; ERLIN2-FGFR1 fusion, 150 kDa.

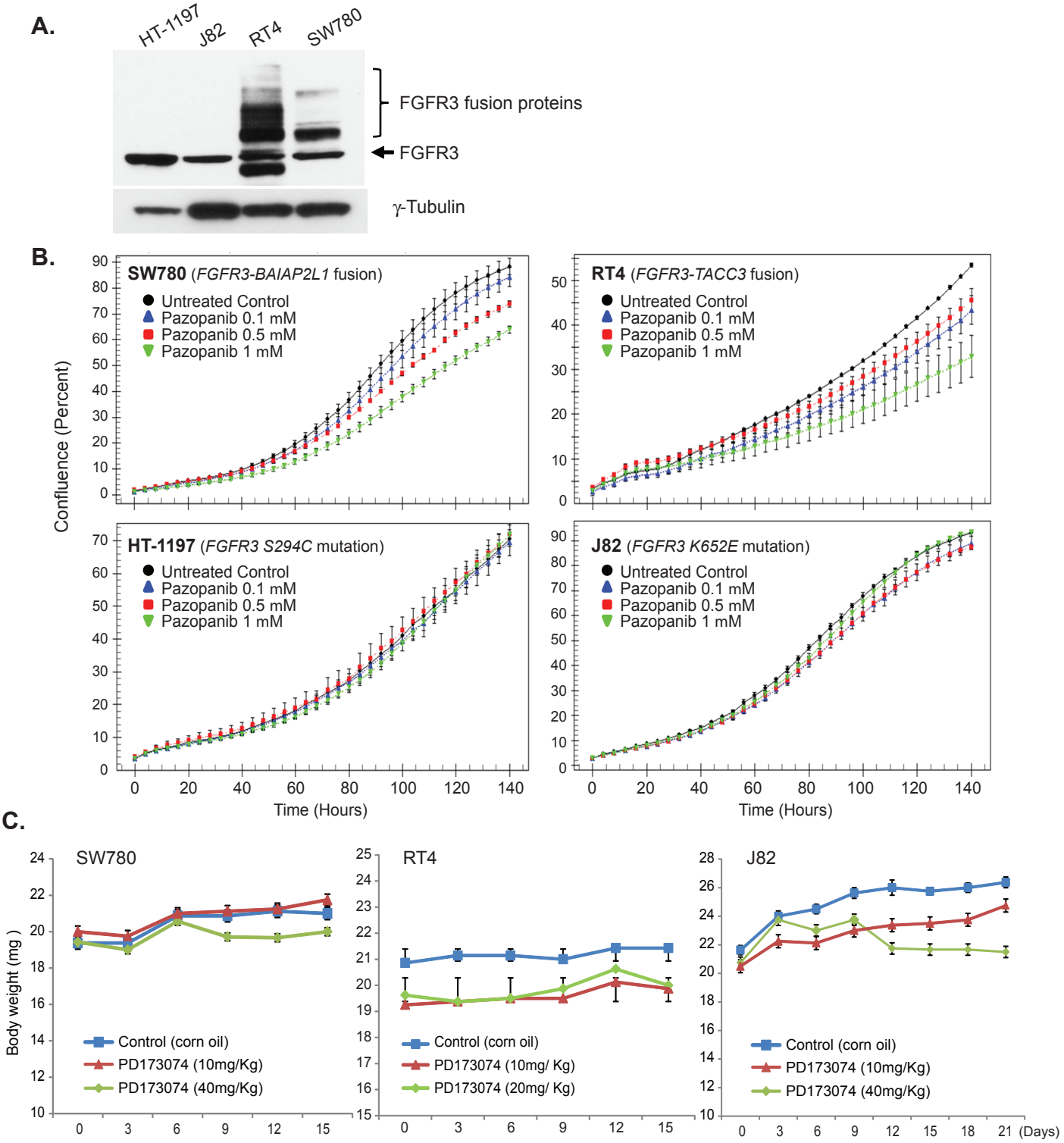

Supplementary Figure S7. **A.** Detection of FGFR3 fusion proteins in bladder cancer cells SW780 (FGFR3-BAIAP2L1) and RT4 (FGFR3-TACC3) by Western blotting. Two control bladder cell lines, J82 (K652E mutation) and HT-1197 (S249C mutation), showed the expression of full length FGFR3. **B.** Differential sensitivity of FGFR fusion positive versus FGFR mutant bladder cancer cancer cell lines to FGFR inhibitor pazopanib. Bladder cancer cells were treated with pazopanib at the indicated concentrations. Cell proliferation assays were determined by Incucyte live-cell imaging. Data shown are cell confluence vs. time at 3 hour intervals. Each data point is the mean of quadruplicates. **C**. Effects of the FGFR inhibitor PD173074 on mouse body weight in xenograft models. Mice xenografted with bladder cancer cell lines SW780, RT4, or J82 were treated daily with two different doses of PD173074 after tumors were formed. Mouse body weight was monitored along with tumor size over a time course of three weeks.

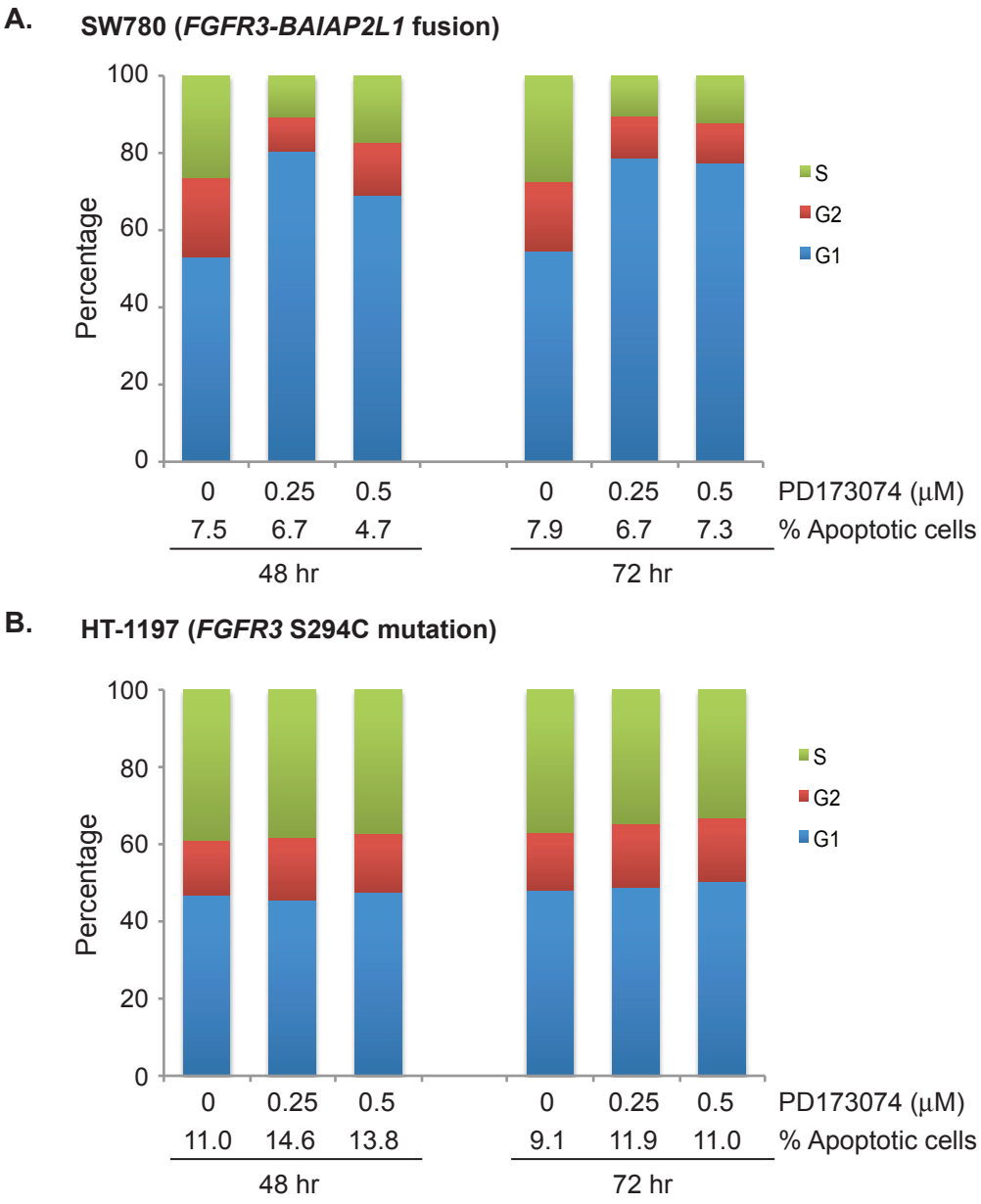

Supplementary Figure S8. Flow cytometry analysis of bladder cancer cells treated with the FGFR inhibitor PD173074. SW780 and HT-1197 cells were treated with 0.25 or 0.5 μM of PD173074 for 48 and 72 hr. Cells were stained with propidium iodide (PI) for cell cycle analysis or FITC-annexin V for apoptosis assays. Percentage distribution of cells in different phases of the cell cycle and the percentage of apoptotic cells are shown.

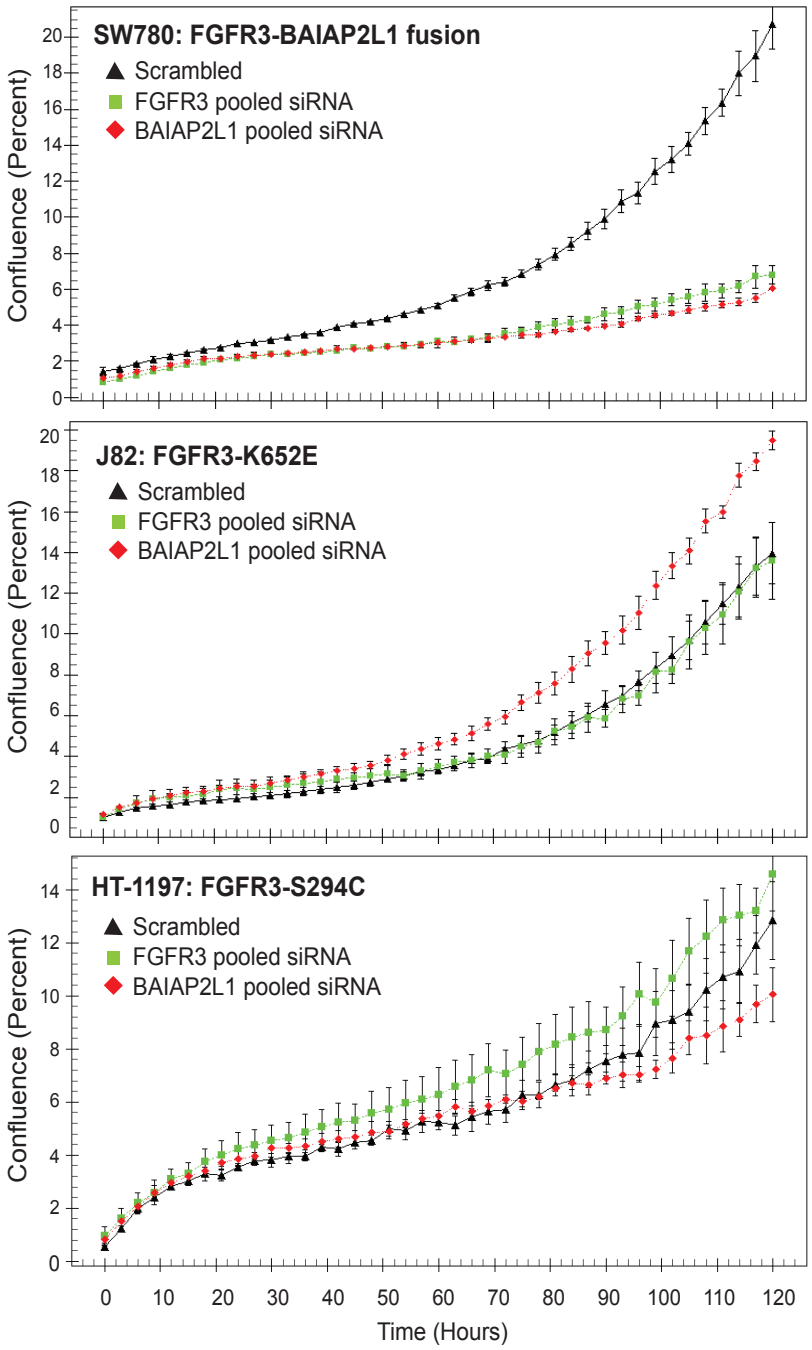

Supplementary Figure S9. Knockdown of *FGFR3* or *BAIAP2L1* reduces proliferation of SW780 cells. Bladder cancer cell lines were transfected with pooled siRNAs targeting either *FGFR3* or *BAIAP2L1*. Cell proliferation assays were determined by Incucyte live-cell imaging. Data shown are cell confluence vs. time at 3 hour intervals. Each data point is the mean of triplicates. In contrast to the FGFR3 fusion-positive SW780cells, the proliferation rates of FGFR3 fusion-negative cells (J82 and HT-1197) were not affected by knockdown of *FGFR3* or *BAIAP2L1*.